Temporal linear stability analysis of an entry flow in a channel with viscous heating

Harshal Srivastava, Amaresh Dalal, Kirti Chandra Sahu† and Gautam Biswas[a]

Department of Mechanical Engineering Indian Institute of Technology Guwahati, Guwahati 781039, India

†*Department of Chemical Engineering, Indian Institute of Technology Hyderabad, Sangareddy: 502 285 Hyderabad, Telangana, India*

(Dated: December 6, 2016)

Abstract

A non-isothermal flow in the entry region of a straight channel in the presence of viscous heating is investigated via direct numerical simulations and a temporal linear stability analysis. Initially, the system is maintained at an isothermal state. As the time progresses, the temperature near the channel walls increases, which in turn decreases the viscosity of the working fluid. This resulting viscosity-stratification in the flow gives rise to an unexpected stability behaviour. From the linear stability analysis, we found that viscous heating has a destabilising influence, and the flow becomes linearly unstable to infinitesimal small disturbance near the developing region of the channel. We also found that increasing the Reynolds number and decreasing the Prandtl number enhance the instability behaviour. For the parameter values considered, the Grashof number does not change the stability characteristics qualitatively. These findings may be relevant to several industrial applications, such as lubrication, tribology, food processing, instrumentation, and polymer processing, to name a few.

[a] gtm@iitg.ernet.in

I. INTRODUCTION

The dynamics of viscous fluid flows through channels/pipes with temperature-dependent viscosity is of great interest in many industrial applications, such as, lubrication, tribology, food processing, instrumentation, and viscometry. In many situations involving highly viscous fluids, the temperature increases due to the friction between the layers of working fluid. This leads to profound changes in the flow structure due to the strong coupling between the energy and momentum equations through temperature dependent viscosity [1–8]. This phenomenon is commonly known as viscous heating [9], which is also known to play an important role in polymer processing industries [10].

Several researchers have investigated the effect of temperature-dependent fluid viscosity and wall heating on flow stability in a variety of configurations, such as, boundary-layer [11, 12], Couette [13, 14], channel [15–18], pipe flows [19, 20] and porous media [21–23]. Although, these authors, among several others, investigated non-isothermal flows, the effect of viscous heating was not considered by them. Next, we review some specific literatures involving viscous heating.

The effect of viscous heating has been studied in Couette and Taylor-Couette flows via linear stability analyses [4, 24, 25] and experimental observations [26]. The main finding of these studies is that increasing viscous heating stabilises the flow by decreasing the 'critical' Reynolds number (the minimum Reynolds number at which the flow is linearly unstable). The stabilising influence of viscous heating was attributed to the coupling between the velocity perturbations and the base state temperature gradient. In a symmetrically-heated channel, Pinarbasi et al. [27] showed that viscous heating destabilises an inelastic fluid flow. Costa et al. [6] also studied the effect of viscous heating in a symmetrically-heated channel flow of a viscous fluid with temperature-dependent viscosity by conducting a linear stability analysis and direct numerical simulations. They showed the appearance of secondary rotational flows due to the influence of viscous heating. Recently, Sahu et al. [28] performed a linear stability analysis for a flow in an asymmetrically-heated channel and found that viscous heating has a destabilising influence. Note that, as all the above-mentioned papers studied the effect of viscous heating on flows with heated walls, they used a fixed temperature at the boundaries. However, such a boundary condition (fixed temperature) at the walls is unphysical in the present context, as the temperature at the walls is expected to

increase continuously due to the heat produced by the viscous heating.

Another aspect to be discussed in the present context is the effect of entry region on the flow characteristics. It is well known that in both isothermal and non-isothermal flows, the assumption of fully-developed flow could obscure the complete route to turbulence [29, 30]. Even for flows in simple geometries, such as isothermal channel/pipe, the distance required to reach a fully-developed state can be very long, and which increases with the increase in Reynolds number. Sahu & Govindarajan [30] conducted linear stability analysis of a flow in the entry region of a straight pipe and found that the flow becomes unstable at a finite Reynolds number, although a fully-developed flow in a straight pipe is linearly stable at any Reynolds number. Nishi *et al.* [31] also observed "puff" flows at lower Reynolds number ($Re \leq 2300$). They observed "puff" splitting with increasing Reynolds numbers. The split "puffs" were developed into "slugs". The investigation showed that the minimum critical Reynolds number required to cause transition is 1940.

In all the previous studies involving viscous heating [6, 28], a well-defined fully-developed flow and a fixed (isothermal) temperature condition at the walls were used. The present work is different from the above-mentioned investigations in two ways. First, unlike the previous studies, we obtained the basic state profiles by conducting direct numerical simulations using a Neumann boundary condition for temperature at the wall, i.e the wall-temperature is allowed to increase to the viscous dissipation. Secondly, the stability analysis is performed for the basic states at different times and spatial locations, which are obtained by solving the Navier-Stokes, energy and continuity equations simultaneously. As expected, the flow does not reach a fully-developed state due to the continuous increase in temperature near the walls due to the viscous heating phenomenon. In this study, we ask a fundamental question, i.e can viscous heating destabilise the entry flow in a straight channel?

The rest of this paper is organised as follows. The problem is formulated in Section II, wherein the basic state and linear stability analysis are discussed. The results of the linear stability analysis are presented in Section III. Concluding remarks are provided in Section IV.

II. FORMULATION

A pressure-driven two-dimensional flow of a highly viscous, Newtonian and incompressible fluid in the entry region of a straight channel with viscous heating is considered. The schematic diagram of the flow configuration is shown in Fig. 1. An uniform flow is imposed at the inlet, which is allowed to develop due to the effect of viscosity along the downstream of the channel. There is no imposed temperature at the wall, i.e. initially the system is at an isothermal state (maintained at a reference temperature T_l). Temperature profile develops due to viscous heating (rubbing of fluid layers in the viscous liquid). A Cartesian coordinate system, (x, y), is deployed to model the flow, wherein x and y denote the streamwise and vertical coordinates, respectively. The rigid and impermeable channel walls are located at $y = \pm H$. The inlet and outlet of the channel are present at $x = 0$ and L, respectively.

The following constitutive equation [8, 24, 32] is used model the viscosity-temperature dependency:

$$\mu_T = \mu_l \exp\left[-\frac{\beta(T_T - T_l)}{T_l}\right]. \tag{1}$$

This model approximates the variation of viscosity of many liquids over a wide range of temperature. Here, μ_l is the value of the viscosity at the reference temperature T_l, and β is a dimensionless activation energy parameter, which is positive for liquids and negative for gases. In the present study, $\beta > 0$ as we deal with a highly viscous liquid.

The following scaling is employed in order to render these equations dimensionless:

$$(x, y) = H\,(\widetilde{x}, \widetilde{y})\,,\ t = \frac{H}{U_m}\widetilde{t},\ (U, V) = U_m(\widetilde{U}, \widetilde{V}),\ P = \rho {U_m}^2 \widetilde{P},$$
$$T_T = \frac{\widetilde{T}_T T_l}{\beta} + T_l,\ \mu_T = \widetilde{\mu}_T \mu_l, \tag{2}$$

where U and V denote the streamwise and vertical velocity components, and P, T_T, ρ and t denote pressure, temperature, density and time, respectively. The tildes designate dimensionless quantities, and $U_m (\equiv Q/2H)$ is the imposed uniform velocity at the inlet, wherein Q is the volume flow rate per unit width in the spanwise direction. With the Boussinesq approximation, the dimensionless governing equations (after dropping tildes from all non-dimensional terms) are given by

$$\frac{\partial U}{\partial x} + \frac{\partial V}{\partial y} = 0, \tag{3}$$

$$\frac{\partial U}{\partial t}+U\frac{\partial U}{\partial x}+V\frac{\partial U}{\partial y}=-\frac{\partial P}{\partial x}+\frac{1}{Re}\left\{\frac{\partial}{\partial x}\left[2\mu_T\frac{\partial U}{\partial x}\right]+\frac{\partial}{\partial y}\left[\mu_T\left(\frac{\partial U}{\partial y}+\frac{\partial V}{\partial x}\right)\right]\right\}, \quad (4)$$

$$\frac{\partial V}{\partial t}+V\frac{\partial V}{\partial x}+V\frac{\partial V}{\partial y}=-\frac{\partial P}{\partial y}+\frac{1}{Re}\left\{\frac{\partial}{\partial x}\left[\mu_T\left(\frac{\partial U}{\partial y}+\frac{\partial V}{\partial x}\right)\right]+\frac{\partial}{\partial y}\left[2\mu_T\frac{\partial V}{\partial y}\right]\right\}+\frac{Gr}{Re^2}T_T, \quad (5)$$

$$\frac{\partial T_T}{\partial t}+U\frac{\partial T_T}{\partial x}+V\frac{\partial T_T}{\partial y}=\frac{Na}{RePr}\mu_T\left[2\left\{\left(\frac{\partial U}{\partial x}\right)^2+\left(\frac{\partial V}{\partial y}\right)^2\right\}+\left(\frac{\partial U}{\partial y}+\frac{\partial V}{\partial x}\right)^2\right]+\frac{1}{RePr}\left[\frac{\partial^2 T_T}{\partial x^2}+\frac{\partial^2 T_T}{\partial y^2}\right]. \quad (6)$$

These equations are coupled via the temperature dependence of the viscosity (given by Eq. 1). The dimensionless form of Eq. 1 is given by

$$\mu_T=\mu_l\exp(-T_T). \quad (7)$$

The dimensionless term associated with viscous heating is the Nahme number, $Na(\equiv \beta\mu_l U_m^2/\kappa T_l)$. Several researchers also use the Brinkman number ($Br\equiv\mu_l U_m^2/\kappa T_l$) to describe viscous heating, which can be defined as Na/β. Increasing the Nahme number increases the extent of coupling of the governing equations. The other dimensionless numbers appearing in Eqs. (3)-(6) are the Reynolds number $Re(\equiv \rho U_m H/\mu_l)$, the Prandtl number $Pr(\equiv c_p\mu_l/\kappa)$ and the Grashof number $Gr(\equiv \alpha_0 T_l g H^3/\beta\nu^2)$. Here, $\nu(\equiv\mu_l/\rho)$ is the kinematic viscosity, while κ, c_p, g and α_0 are coefficient of thermal conductivity, specific heat capacity at constant pressure, the acceleration due to gravity and the thermal expansion coefficient, respectively.

In order to perform a localised temporal stability analysis, the flow variables are expressed as the sum of the basic state variables at a given streamwise position and time-dependent perturbations:

$$(U,V,P,T_T,\mu_T)(x,y,t)=(U_0,V_0,P_0,T_0,\mu_0)(y)|_x+\left(\hat{u},\hat{v},\hat{p},\hat{T},\hat{\mu}\right)(x,y,t), \quad (8)$$

where the subscripts 0 and hats represent the basic state quantities and the perturbations, respectively. In the next subsection, we discuss the computational method used to obtain the basic state.

A. Basic state

The basic state is obtained by solving Eqs. (3)-(6) directly in the computational domain shown in Fig. 1. The numerical method used is briefly discussed below. Initially (at

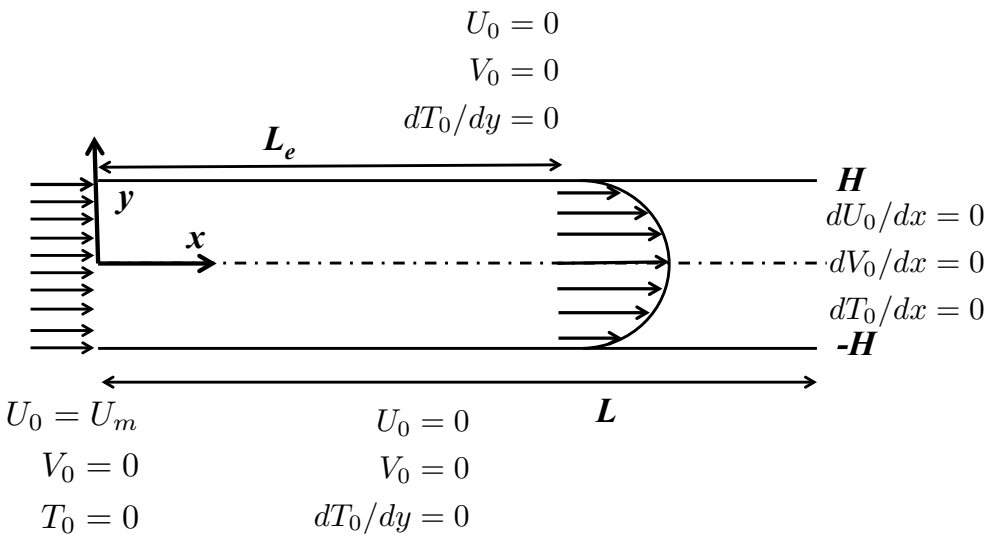

FIG. 1. Schematic diagram of developing flow in the entry region of a channel (not to scale). The aspect ratio of the channel, L/H is 60.

$t = 0$), the dimensionless velocity components and temperature are set to zero throughout the domain. At $t \geq 0$, the dimensionless velocity $(U_0, V_0) = (1, 0)$ is imposed at the inlet of the channel ($x = 0$). No-slip and no-penetration boundary conditions are imposed at the top and bottom walls. Due to the viscous heating the temperature of the working fluid increases with time as the flow develops in the downstream direction. A Neumann boundary condition for temperature is imposed at the walls, which implies that the walls are infinitely conducting. Neumann boundary conditions for velocity components and temperature are used at the outlet of the channel.

In order to resolve the high shear region, where the viscous heating term dominates, a non-uniform grid in the y direction that refines the mesh near the solid boundaries, is used in our simulations. This is achieved by using the following grid:

$$y_{i,j} = -cos\left(\frac{\pi(j-1)}{N-1}\right), \tag{9}$$

where (i, j) denote the grid numbering in the streamwise and vertical directions, respectively. A uniform grid is used in the streamwise direction. A grid convergence test is conducted and an optimal grid (601 and 101 grid points in the x and y directions) by balancing the computational time and accuracy of the results is obtained. This is used in generating all the results presented in this study. We have checked our basic state velocity and temperature profiles obtained from two computational domains, namely, $L/H = 60$ and 100, and

found that the profiles obtained using these computational domains match perfectly in the developing flow regime.

The discretised Eqs. (3)-(6) are solved using MAC (Marker and Cell) algorithm, which involves the calculations of basic state velocity components using the best possible value of pressure and previous values of the other variables obtained at the previous iteration. The pressure correction equation is solved iteratively using an efficient *"Bi-CGstab with SIP as preconditioner"* solver, which is obtained by substituting the velocity components in the continuity equation, Eq. (3). At every time step, iterations are performed till the residue reduces to the prescribed limit (here it is 10^{-8}). Using the resultant velocity components, Eq. (6) is solved to obtain the temperature field in the next time step. The time step used in our numerical simulation is 10^{-4}.

Typical basic state profiles of the streamwise and vertical velocity components and temperature profiles at $t = 100$ are plotted at different x locations in Fig. 2(a), (b) and (c), respectively. The rest of the parameter values are $Re = 2000$, $Na = 30$, $Pr = 1$ and $Gr = 0$. It can be seen in Fig. 2(a) that the maximum velocity in the center region of the channel increases as we move in the downstream direction. In order to satisfy the continuity equation, the vertical velocity, which is maximum near the top and bottom walls at any given streamwise location, decreases as we move in the positive x direction. The velocity profiles are influenced by the decrease in viscosity of the fluid, due to the increase in temperature in the near wall regions because of viscous heating. It can be seen in Fig. 2(c) that a boundary layer for temperature develops near the walls, which grows along the streamwise direction. This behaviour can also be seen in Fig. 3, which shows a spatio-temporal evolution of temperature for the parameter values the same as those used to generate Fig. 2.

B. Linear stability analysis

In this section, we formulate the temporal linear stability equations. As the flow is continuously evolving due to the influence of viscous heating, we used a pseudo-steady state type approach and perform linear stability analysis of the basic state profile at a few specific streamwise locations. Using a normal modes analysis, the infinitesimal, two-dimensional (2D) perturbations are expressed as [29],

$$(\hat{u}, \hat{v}, \hat{p}, \hat{T}, \hat{\mu})(x, y, t) = (u, v, p, T, \mu)(y) \exp\left(\mathrm{i}\left[\alpha x - \omega t\right]\right), \tag{10}$$

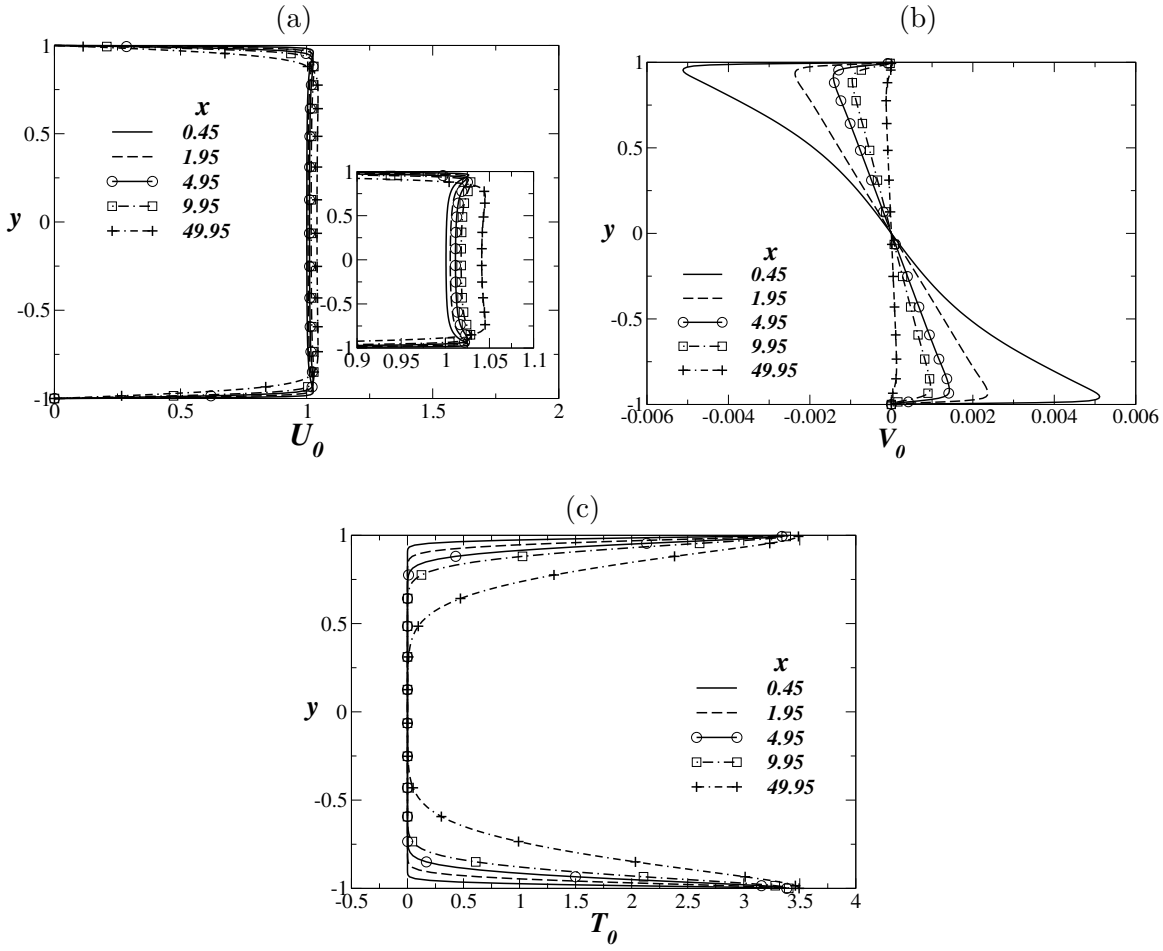

FIG. 2. Typical profiles of streamwise, vertical velocity components and temperature at $t = 100$ at different streamwise locations. The inset in panel (a) represents the zoomed view of streamwise velocity profiles. The rest of the parameter values are $Re = 2000$, $Na = 30$, $Pr = 1$ and $Gr = 0$.

In Eq. (10), $\hat{\mu} = (d\mu_0/dT_0)\,\hat{T}$ represents the perturbation viscosity, and α is the disturbance wavenumber (real). $\omega(\equiv \omega_r + \mathrm{i}\omega_i)$ is a complex frequency, wherein ω_r and ω_i represent the real and imaginary parts. The amplitude of the velocity disturbances are re-expressed in terms of a streamfunction: $(\hat{u}, \hat{v}) = (\psi', -\mathrm{i}\alpha\psi)$, where the prime denotes differentiation with respect to y. Substitution of Eqs. (8) and (10) into Eqs. (3)-(6), followed by subtraction of the base state equations, subsequent linearization and elimination of the pressure perturbation yields the following linear stability equations:

$$\mathrm{i}\alpha\left[\left(\psi'' - \alpha^2\psi\right)(U_0 - c) - \psi U_0''\right] = \frac{1}{Re}\Big[\mu_0\left(\psi'''' - 2\alpha^2\psi'' + \alpha^4\psi\right) + 2\frac{d\mu_0}{dT_0}T_0'\left(\psi''' - \alpha^2\psi'\right) +$$

$$\frac{d\mu_0}{dT_0}T_0''\left(\psi'' + \alpha^2\psi\right) + \frac{d^2\mu_0}{dT_0^2}\left(T_0'\right)^2\left(\psi'' + \alpha^2\psi\right) + \frac{d\mu_0}{dT_0}\left(U_0'T'' + 2U_0''T' + \alpha^2U_0'T + U_0'''T\right) +$$

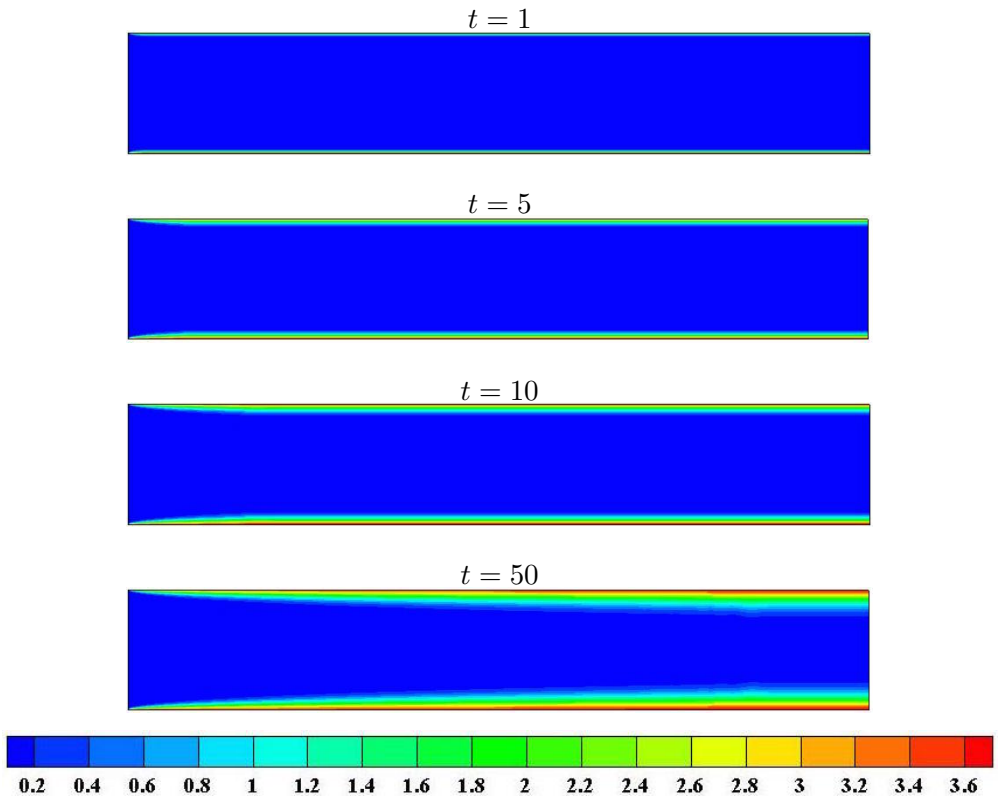

FIG. 3. Spatio-temporal evolution of temperature distribution for $Re = 2000$, $Na = 30$, $Pr = 1$ and $Gr = 0$.

$$2\frac{d^2\mu_0}{dT_0^2}T_0'U_0'T' + \frac{d^2\mu_0}{dT_0^2}T_0''U_0'T + \frac{d^3\mu_0}{dT_0^3}\left(T_0'\right)^2 U_0'T + 2\frac{d^2\mu_0}{dT_0^2}T_0'U_0''T\Big] - \frac{Gr}{Re^2}\mathrm{i}\alpha T, \tag{11}$$

$$\mathrm{i}\alpha\left[(U_0 - c)T - \psi T_0'\right] = \frac{1}{RePr}\left[T'' - \alpha^2 T\right] + \frac{Na}{RePr}2U_0'\mu_0\left(\psi'' + \alpha^2\psi\right), \tag{12}$$

where $c\,(\equiv \omega/\alpha)$, is a complex phase speed of the disturbance. Note that a given mode is unstable if $\omega_i > 0$, stable if $\omega_i < 0$ and neutrally stable if $\omega_i = 0$. It can be seen that in the limit $(Na \to 0)$, these equations reduce to those of Sameen *et al.* [16]; and in the limit $(Na, Gr) \to 0$, we obtained the stability equations of Wall *et al.* [17]. We can also recover the classical Orr-Sommerfeld equation by setting $T_0 = 0$ and $\mu_0 = 1$ (i.e for an isothermal configuration).

The boundary conditions for the perturbation quantities are

$$\psi = \psi' = T' = 0 \quad \text{at} \quad y = \pm 1. \tag{13}$$

Eqs. (11) and (12) along with these boundary conditions constitute an eigenvalue problem,

which can be written in the matrix form as

$$\begin{bmatrix} \mathcal{A}_{11} & \mathcal{A}_{12} \\ \mathcal{A}_{21} & \mathcal{A}_{22} \end{bmatrix} \begin{bmatrix} \psi \\ T \end{bmatrix} = c \begin{bmatrix} \mathcal{B}_{11} & \mathcal{B}_{12} \\ \mathcal{B}_{21} & \mathcal{B}_{22} \end{bmatrix} \begin{bmatrix} \psi \\ T \end{bmatrix}. \tag{14}$$

We use the same discretisation (Eq. 9) as that used for the basic state calculations. The eigenvalue problem is then solved using the public domain software, LAPACK [29].

III. RESULTS AND DISCUSSION

The results obtained from the above linear stability analysis are discussed in this section. Particular attention will be given to the effect of varying the Nahme number. The effects of other dimensionless parameters, such as the Reynolds number, Prandtl number and Grashof number on the linear stability characteristics of flow in the presence of viscous heating have also been discussed.

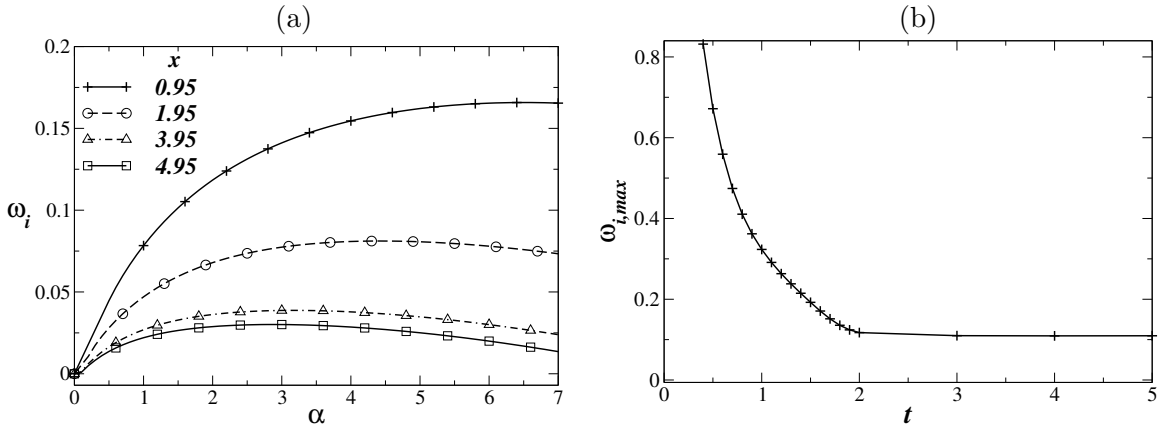

FIG. 4. (a) Dispersion curves (ω_i versus α) at different streamwise locations at $t = 50$. (b) The variation of maximum growth rate, $\omega_{i,max}$ with time at $x = 1.45$. The rest of the parameter values are $Re = 2000$, $Pr = 1$, $Gr = 0$ and $Na = 30$.

In Fig. 4(a), we plot dispersion curves (ω_i versus α) for the numerically generated basic state profiles at different x locations at $t = 50$. The other parameters of interest in this plot are $Re = 2000$, $Pr = 1$, $Gr = 0$ and $Na = 30$. It can be seen that dispersion curves depicted in Fig. 4(a) are paraboloidal, and $\omega_i > 0$ over a finite band of wavenumbers, indicating the presence of a linear instability. It can also be seen that there is a well-defined "most-dangerous" mode that corresponds to the value of α for which ω_i is maximal.

Although it is not shown for all x locations, ω_i becomes negative (flow becomes stable) for large α. The value of ω_i of the "most-dangerous" mode is designated by $\omega_{i,max}$. It can be seen that the flow is more unstable near the entrance region, and the growth rate of the "most-dangerous" mode decreases as we move in the downstream direction. In Fig. 4(b), the variation of $\omega_{i,max}$ with time is plotted at $x = 1.45$. It can be seen that the growth rate of the "most-dangerous" mode decreases with time, and reaches to a plateau for $t > 2$ for this set of parameters. We found a similar trend (not shown) for other set of parameters too. The result shown in Fig. 4(b) justifies the assumption of pseudo-steady state made in this study.

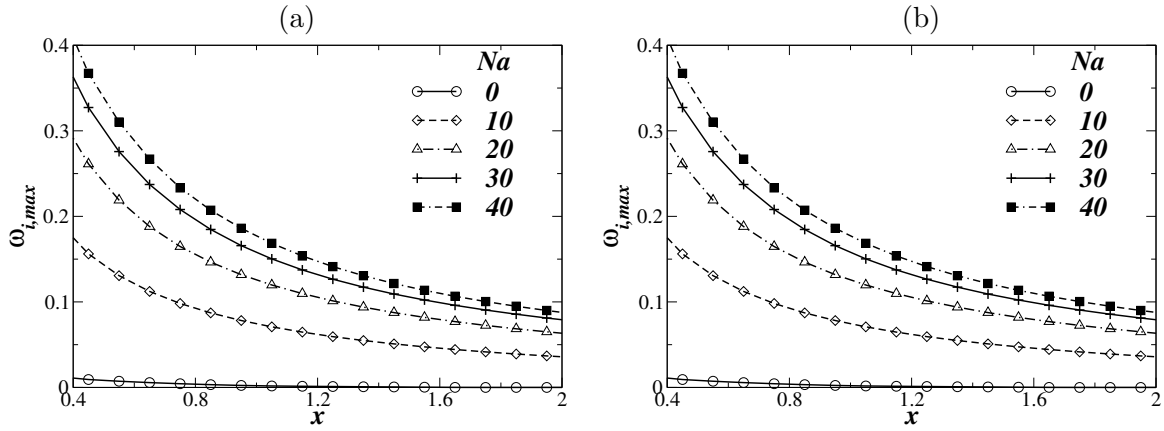

FIG. 5. The variation of $\omega_{i,max}$ versus x for different values of Na at (a) $t = 50$ and (b) $t = 100$. The rest of the parameter values are $Re = 2000$, $Pr = 1$ and $Gr = 0$.

We investigate the effect of Nahme number, i.e. influence of viscous heating on the linear stability characteristics in Fig. 5. The variations of $\omega_{i,max}$ along the downstream direction is plotted for different values of Na at $t = 50$ and $t = 100$ in Fig. 5(a) and (b), respectively for $Re = 2000$, $Pr = 1$ and $Gr = 0$. It can be seen that the growth rate of the "most-dangerous" mode is maximum near the entrance of the channel, where the streamwise velocity is almost uniform, but the vertical velocity is maximum near the walls. It can be seen that $\omega_{i,max}$ decreases as we move in the downstream direction. It is to be noted here that the maximum vertical velocity also decreases along the positive x direction. Thus it appears that the vertical velocity, which in turn creating a curvature in the streamwise velocity profile near the centerline region, is destabilising the flow. It can be seen that increasing Na, which is equivalent to increase the extent of viscous heating, increases the value of $\omega_{i,max}$ at any given

location. This indicates that the viscous heating is destabilising the flow in the developing region. This finding is consistent with that of Sahu et al. [28]; however, contradict the dogma that viscous heating has a stabilising influence [4, 24, 25]. As discussed above, it can be seen in Fig. 5(b) that the variations of $\omega_{i,max}$ versus x at $t = 100$ look similar to those at $t = 50$ (shown in Fig. 5(a)).

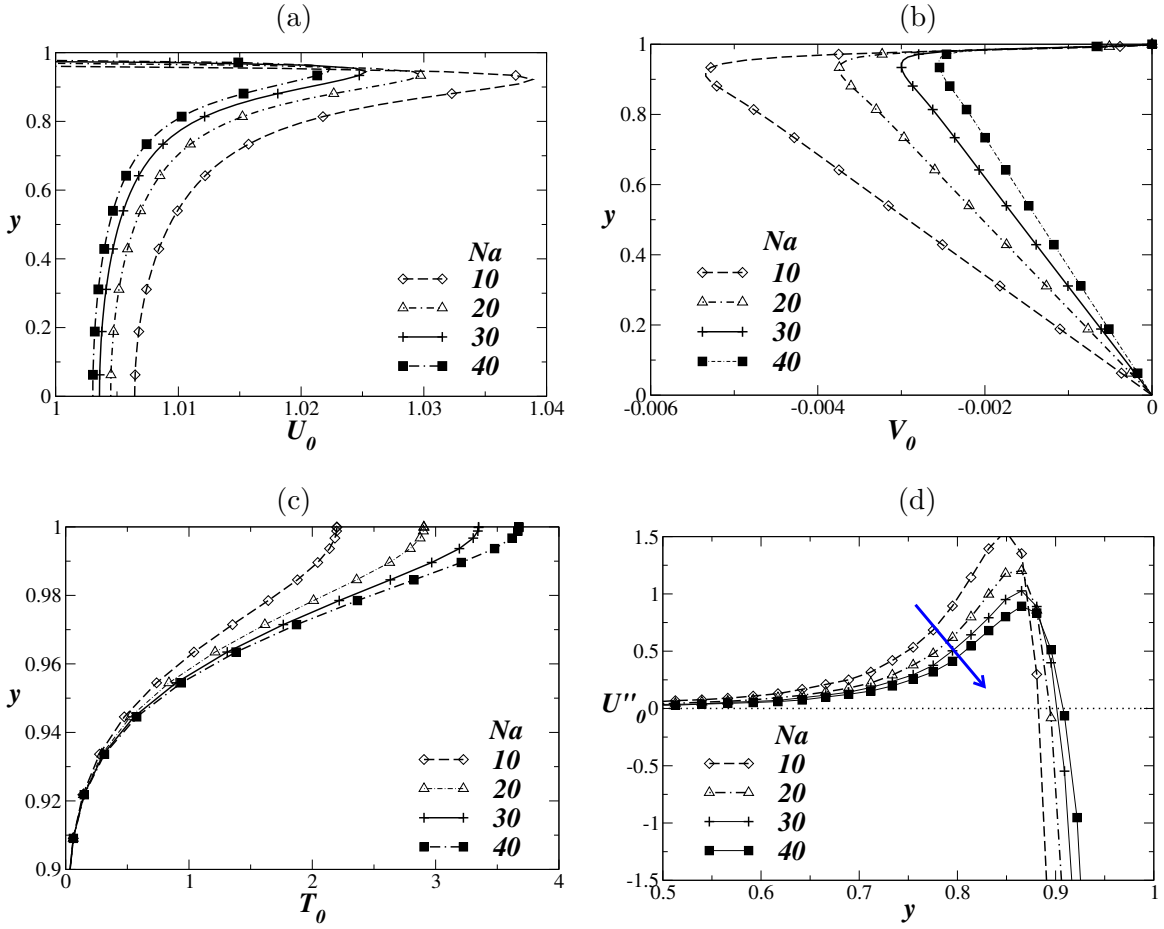

FIG. 6. Basic state profiles of (a) U_0, (b) V_0, (c) T_0 and (d) $U_0{}''$ for different Na at $x = 1.25$. The rest of the parameter values are the same as those used to generate Fig. 5.

In order to get insight of the destablising mechanism of the Nahme number, we have plotted basic state profiles of U_0, V_0, T_0 and $U_0{}''$ for different values of Na in Fig. 6(a), (b), (c) and (d), respectively. As these profiles are symmetrical, we show them only in the upper part of the channel. It can be seen in Fig. 6(a) and (b) that increasing Na decreases the boundary layer thickness, which can be inferred from the shifting of the location of maximum value of U_0 and minimum value of V_0 towards the top wall. A similar effect is also seen near the bottom wall (not shown). This is due to the fact that increasing Na increases the walls

temperature, which in turn decreases the viscosity of the fluid in the near wall regions. As the effect of viscosity is only confined to the thin near-wall regions, we thought that inviscid mechanism could be operational, which is indeed the case for adverse pressure-gradient boundary layer and channel flows [9, 29]. The inflection point criteria (Reyleigh's inviscid stability theorem [33]) states that for a flow to be inviscidly unstable, the basic state profile should have an inflection point ($U_0{}'' = 0$). Thus, we have plotted a zoomed figure showing the variation of $U_0{}''$ across the channel from $0.5 \leq y \leq 1$. However, we can see that the instability mechanism is not inviscid. This can be inferred from Fig. 6(d), which shows that increasing Na brings the $U_0{}''$ closer to $U_0{}'' = 0$ line (shown by the arrow mark in Fig. 6(d)). This means that increasing Na decreases the inflectional behaviour of the velocity profile. On the other hand, due to the viscosity stratification generated because of viscous heating, the boundary layer becomes thinner than that in the corresponding isothermal system. This in turn, increases the gradient of velocity components (increases the shear-stress) near the walls, which might have played a role in destabilising the flow.

In order to understand this further, in Fig. 7(a), (b), (c) and (d), we plot the variations of the real and imaginary parts of ψ and T eigenfunctions in the wall-normal direction for different values of Na. The value of wave number considered ($\alpha = 4.5$) corresponds to a typical value of wave number close to the most dangerous modes for all values of Na. The basic velocity and temperature profiles at $x = 0.95$ are used to generate Fig. 7. The rest of the parameter values are the same as those used for Fig. 5. It can be seen that increasing the value of Na increases the maximum values of the real (ψ_r) and imaginary (ψ_i) parts of the perturbed streamfunction. We can also observe that although the basic temperature profile has a maximum near the wall due to the effect of viscous heating, the resultant temperature perturbations concentrated near the centre of the channel (Fig. 7(c) and (d)). Close inspection also reveals that the maxima of the perturbed streamfunction and temperature profiles shifted towards the centerline with the increase in the level of viscous heating.

Then we investigate the effects of the Reynolds number, Prandtl number and Grashof number on the stability characteristics of the flow in the presence of viscous heating in Fig. 8(a), (b) and (c), respectively. We chose a typical value of the Nahme number ($Na = 30$) to generate this figure. It can be seen in Fig. 8(a) that increasing the Reynolds number has a destabilising influence. It is expected as keeping the the flow rate and geometry fixed,

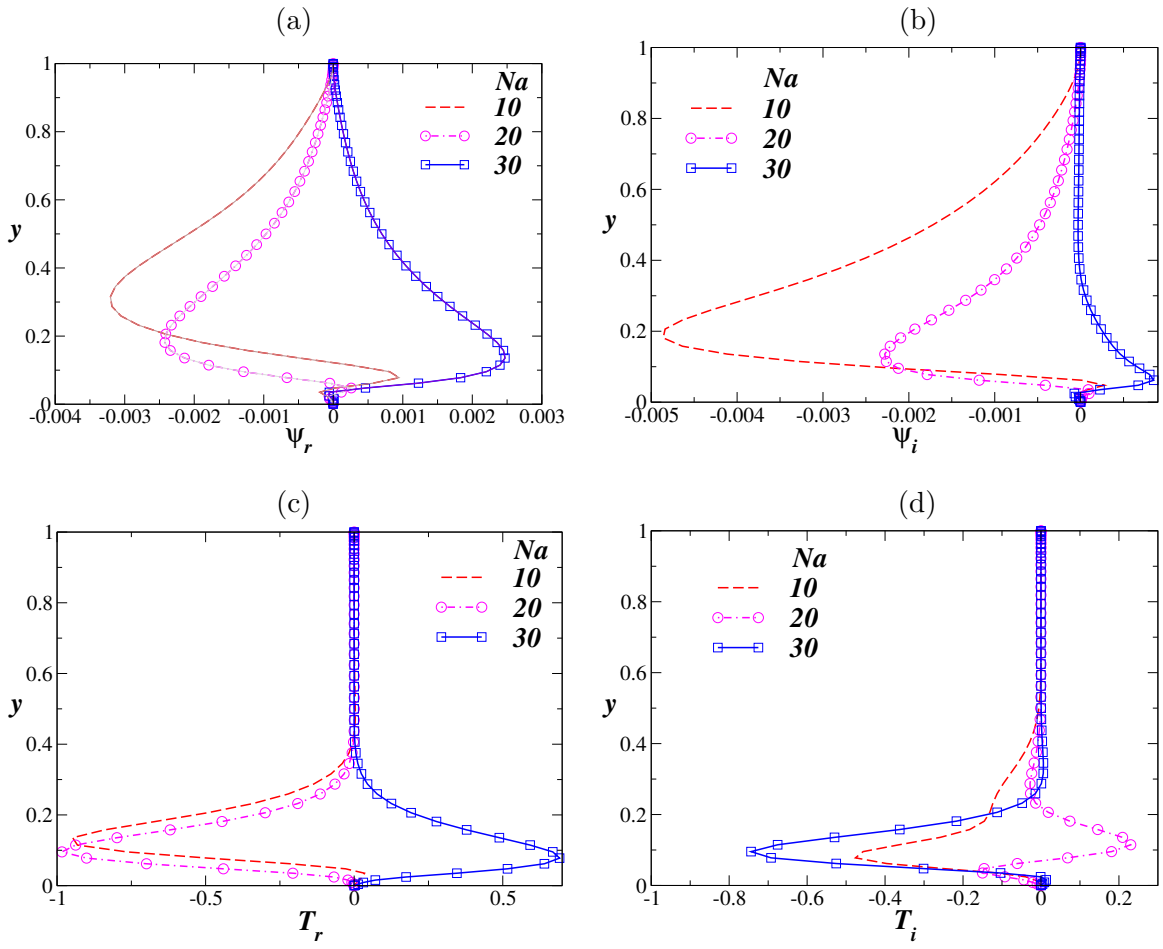

FIG. 7. The real (a,c), and imaginary (b,d) parts of ψ (a,b) and T (c,d) eigenfunctions for $\alpha = 4.5$ for different values of Na. The basic velocity and temperature profiles at $x = 0.95$ for $t = 50$ are used to generate these plots. The rest of the parameter values are the same as those used to generate Fig. 5.

increasing the Reynolds number means decreasing the viscosity of the fluid. Thereby, decreasing the thickness of the momentum boundary layer, but increasing the thickness of the temperature boundary layer (for a fixed value of Na). The combined effect of these phenomena destabilises the flow dynamics in this case. It can be seen in Fig. 8(b) that increasing the Prandtl number (i.e., decreasing the thermal conductivity of the fluid) decreases the maximum growth rate at any streamwise location. The results of the isothermal case (shown by dashed line in Fig. 8(b)) shows that the flow is almost neutrally stable ($\omega_i \approx 0$) for this set of parameter values. As the inertia is high in the flow considered in this study, the Grashof number has a negligible influence on the stability characteristics (as expected),

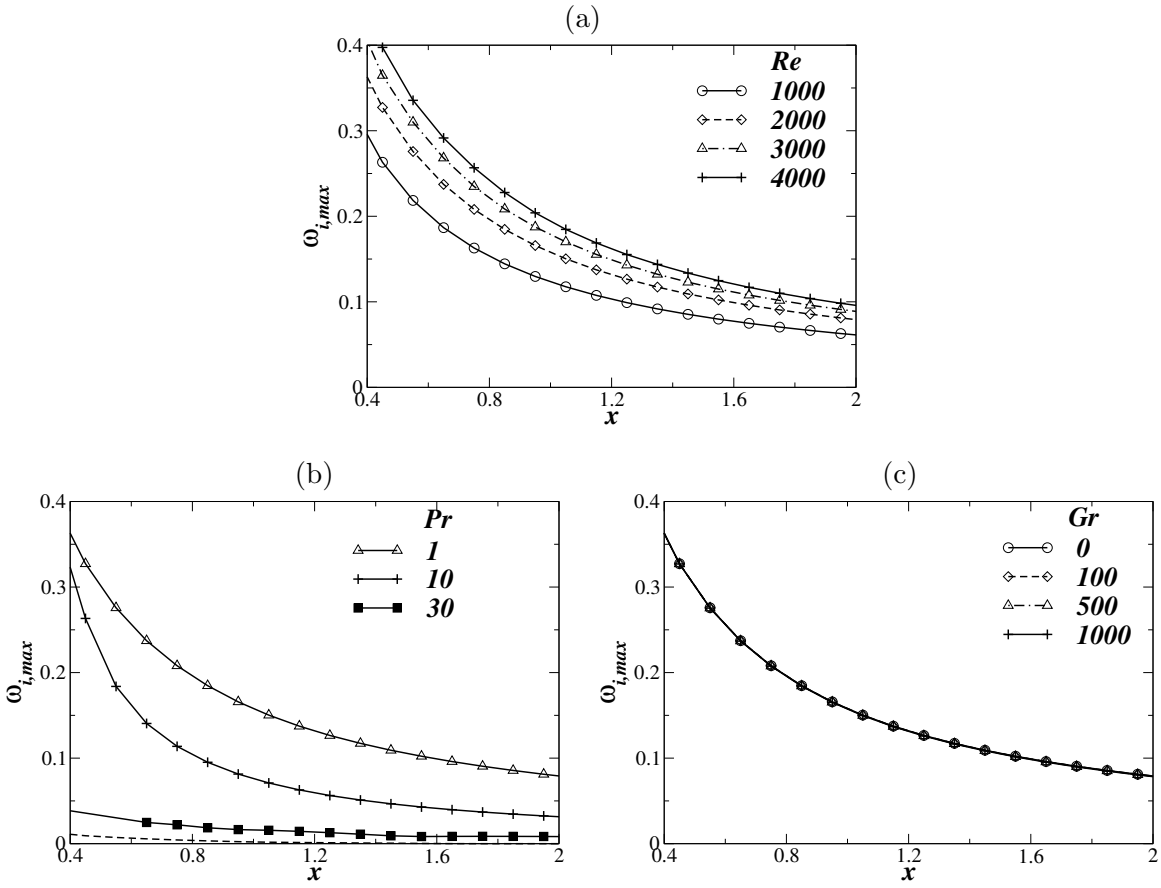

FIG. 8. The variation of $\omega_{i,max}$ versus x at $t = 100$ for different values of (a) Re for $Pr = 1$ and $Gr = 0$, (b) Pr for $Re = 2000$ and $Gr = 0$; in this panel, the result of isothermal case is shown by dashed line, and (b) Grashof number, Gr for $Pr = 1$ and $Re = 2000$. Here, $Na = 30$.

which can be seen in Fig. 8(c).

IV. CONCLUDING REMARKS

A temporal linear stability analysis is conducted to study the flow in entry region of a straight channel in the presence of viscous heating. Unlike the previous studies on this subject, we obtained the basic state profiles by conducting direct numerical simulations of the Navier-Stokes, energy and continuity equations using a Neumann boundary condition for temperature at the walls. All the previous studies, fixed the temperature at the walls, which is unphysical in the present context, as the wall temperature is expected to increase continuously due to the heat generated in the presence of viscous heating. The increase in

fluid temperature near the walls decreases the viscosity of the working liquid, which in turn gives rise to an unexpected stability behaviour. Our linear stability analysis reveals that viscous heating (increasing the Nahme number) has a destabilising influence, and the flow becomes linearly unstable to infinitesimal small disturbance near the developing region of the channel. We also found that increasing the Reynolds number and Prandtl number have destabilising and stabilising effects on the flow, respectively. The variation of the Grashof number does not influence the stability characteristics for the range of parameters considered in the present study. These findings may be useful several industrial applications.

---

[1] J. R. A. Pearson, Variable-viscosity flows in channels with high heat generation, J. Fluid Mech., 83 (1977), pp. 191–206.

[2] H. Ockendon, Channel flow with temperature-dependent viscosity and internal viscous dissipation, J. Fluid Mech., 93 (1979), pp. 737–746.

[3] H. Ockendon and J. Ockendon, Variable-viscosity flows in heated and cooled channels, J. Fluid Mech., 83 (1977), pp. 177–190.

[4] J. J. Wylie and H. Huang, Extensional flows with viscous heating, J. Fluid Mech., 571 (2007), pp. 359–370.

[5] R. Govindarajan and K. C. Sahu, Instabilities in viscosity-stratified flow, Annu. Rev. Fluid Mech., 46 (2014), pp. 331–353.

[6] A. Costa and G. Macedonio, Viscous heating effects in fluids with temperature-dependent viscosity: triggering of secondary flows, J. Fluid Mech., 540 (2005), pp. 21–38.

[7] A. Pinarbasi and C. Ozalp, Influence of variable thermal conductivity and viscosity for non-isothermal fluid flow, Phys. Fluids, 17 (2005), p. 038109.

[8] A. Pinarbasi and C. Ozalp, Effect of viscosity models on the stability of a non-Newtonian fluid in a channel with heat transfer, Int. Comm. Heat Mass Transfer, 28 (2001), pp. 369–378.

[9] F. M. White, *Viscous Fluid Flow*, 2 ed. (McGraw-Hill, Inc., ADDRESS, 1991).

[10] J. R. A. Pearson, *Mechanics of polymer processing* (Elsevier, London, 1985).

[11] D. J. Tritton, Transition to turbulence in the free convection boundary layers on an inclined heated plate, J. Fluid Mech., 16 (1963), pp. 417–435.

[12] J. Hu, H. Ben Hadid, D. Henry, and A. Mojtabi, Linear temporal and spatio-temporal stability analysis of a binary liquid film flowing down an inclined uniformly heated plate, J. Fluid Mech., 599 (2008), pp. 269–298.

[13] D. M. Herbert, On the stability of visco-elastic liquids in heated plane Couette flow, J. Fluid Mech., 17 (1963), pp. 353–359.

[14] N. T. M. Eldabe, M. F. El-Sabbagh, and M. A.-S. El-Sayed(Hajjaj), The stability of plane Couette flow of a power-law fluid with viscous heating, Phys. Fluid, 19 (2007), p. 094107.

[15] P. Schäfer and H. Herwig, Stability of plane Poiseuille flow with temperature dependent viscosity, Int. J. Heat Mass Trans., 36 (1993), pp. 2441–2448.

[16] A. Sameen and R. Govindarajan, The effect of wall heating on instability of channel flow, J. Fluid Mech., 577 (2007), pp. 417–442.

[17] D. P. Wall and S. K. Wilson, The linear stability of channel flow of fluid with temperature dependent viscosity, J. Fluid Mech., 323 (1996), pp. 107–132.

[18] A. Pinarbasi and A. Liakopoulos, Role of variable viscosity in the stability of channel flow, Int. Comm. Heat Mass Trans., 22 (1995), pp. 837–847.

[19] L. S. Yao, Entry flow in a heated straight tube, J. Fluid Mech., 88 (1978), pp. 465–483.

[20] D. D. Joseph, Variable viscosity effects on the flow and stability of flow in channels and pipes, Phys. Fluids, 7 (1964), pp. 1761–1771.

[21] P. Bera and A. Khalili, Stability of mixed convection in an anisotropic vertical porous channel, Phys. Fluids, 14 (2002), pp. 1617–1630.

[22] M. Bhowmik, P. Bera, J. Kumar, Non-isothermal Poiseuille flow and its stability in a vertical annulus filled with porous medium, Int. J. Heat Fluid Flow, 56 (2015), pp. 272–283.

[23] A. A. Hill and B. Straughan, Stability of Poiseuille Flow in a Porous Medium, Advances in Mathematical Fluid Mechanics, (2009), pp. 287–293.

[24] P. C. Sukanek, C. A. Goldstein, and R. L. Laurence, The stability of plane Couette flow with viscous heating, J. Fluid Mech., 57 (4) (1973), pp. 651–670.

[25] C. S. Yueh and C. I. Weng, Linear stability analysis of plane Couette flow with viscous heating, Phys. Fluids, 8 (1996), pp. 1802–1813.

[26] J. White and S. Muller, Viscous heating and the stability of Newtonian and viscoelastic Taylor-Couette flows, Phys. Rev. Lett., 84 (2000), pp. 5130–5133.

[27] A. Pinarbasi and M. Imal, Viscous heating effects on the linear stability of Poiseuille flow of an inelastic fluid, J. non-Newt. Fluid Mech., 127 (2005), pp. 61–71.

[28] K. C. Sahu and O. K. Matar, Stability of plane channel flow with viscous heating, J. Fluids Eng., 132 (2010), p. 011202.

[29] K. C. Sahu and R. Govindarajan, Stability of flow through a slowly diverging pipe, J. Fluid Mech., 531 (2005), pp. 325–334.

[30] K. C. Sahu and R. Govindarajan, Linear instability of entry flow in a pipe, J. Fluids Eng., 129 (2007), pp. 1277–1280.

[31] M. Nishi, B. Unsal, F. Durst and G. Biswas, Laminar-to-turbulent transition of pipe flows through puffs and slugs, J. Fluid Mech., 614 (2008), pp. 425–446.

[32] R. Nahme, Beiträge zur hydrodynamischen Theorie der Lagerreibung, Ingenieur-Archiv, 11 (1940), pp. 191–209.

[33] L. Rayleigh, On the stability of certain fluid motions, Proc. Lond. Maths. Soc., 11 (1880), pp. 57–70.